NASA Technical Memorandum 103212

Hot Gas Ingestion Characteristics and Flow Visualization of a Vectored Thrust STOVL Concept

Albert L. Johns, George H. Neiner, and Timothy J. Bencic
Lewis Research Center
Cleveland, Ohio

Joseph D. Flood, Kurt C. Amuedo, Thomas W. Strock, and Ben R. Williams
McDonnell Aircraft Company
St. Louis, Missouri

Prepared for the
International Powered Lift Conference
sponsored by the Royal Aeronautical Society
London, United Kingdom, August 29–31, 1990

NASA

HOT GAS INGESTION CHARACTERISTICS AND FLOW VISUALIZATION OF A VECTORED THRUST STOVL CONCEPT

Albert L. Johns, George H. Neiner, and Timothy J. Bencic
National Aeronautics and Space Administration
Lewis Research Center
Cleveland, Ohio 44135-3191

Joseph D. Flood, Kurt C. Amuedo, Thomas W. Strock, and Ben R. Williams
McDonnell Aircraft Company
P.O. Box 516
St. Louis, Missouri 63166-0516

E-5623

Abstract

A 9.2 percent scale short takeoff and vertical landing (STOVL) hot gas ingestion model was designed and built by McDonnell Douglas Corporation (MCAIR) and tested in the NASA Lewis Research Center 9- by 15-Foot Low Speed Wind Tunnel (LSWT). Hot gas ingestion, the entrainment of heated engine exhaust into the inlet flow field, is a key development issue for advanced short takeoff and vertical landing aircraft. This paper covers Phase I test program, conducted by NASA Lewis and McDonnell Douglas Corporation, evaluated the hot ingestion phenomena and control techniques and Phase II test program which was conducted by NASA Lewis. The Phase II program evaluated exhaust nozzles temperatures up to 1460 °R and utilized a sheet laser system for flow visualization of the model flow field in and out of ground effects.

Hot gas ingestion levels were measured for the several forward nozzle splay configuration and with flow control/lift improvement devices which reduced the hot gas ingestion. The model support system had four degrees of freedom, heated high pressure air for nozzle flow, and a suction system exhaust for inlet flow. The headwind (freestream) velocity for Phase I was varied from 8 to 90 kn, with primary data taken in the 8 to 23 kn headwind velocity range. Phase II headwind velocity was varied from 10 to 23 kn.

This paper documents results of both Phase I and II. A description of the model, facility, a new model support system, and a sheet laser illumination system are also provided. Results will be presented over a range of main landing gear height (model height) above the ground plane at a 10 kn headwind velocity.

The exception occurs when the effect of headwind velocity is presented in the Phase I results from 8 to 90 kn. The results contain the compressor face pressure and temperature distortions, total pressure recovery, compressor face temperature rise, and the environmental effects of the hot gas. The environmental effects include the ground plane temperature and pressure distributions, model airframe heating, and the location of the ground flow separation. Results from the sheet laser flow visualization test will also be shown.

Introduction

Advanced short takeoff and vertical landing (STOVL) aircraft are being considered for operation around the turn of the century. In order to meet this target, it is necessary that the technologies critical to the successful operation of the STOVL concepts be resolved. One of the critical technologies associated with the vectored lift concept is that of hot gas ingestion while the aircraft is in ground effect (Refs 1 and 2).

Hot gas ingestion can be categorized as near field and far field phenomena (Fig 1). The near field hot gas problem occurs when two or more hot exhaust jets impinge on the ground and radiate in all directions until

one jet encounters another jet. When these jets meet a fountain is formed. This fountain can hit the undersurface of the fuselage and run forward into the inlet flow field. The hot air, once ingested can result in both compressor temperature and pressure distortions and loss in engine thrust and/or stall. The near field hot gas ingestion is generally the primary source of the hot gas ingestion. The near field hot gas ingestion is a function of the model height above the ground plane (Ref 3). The far field hot gas ingestion occurs when the ground jet from the nozzle(s) flow separates from the ground ahead of the model and gets blown back into the inlet flow field. The far field hot gas ingestion is a function of the headwind velocity. The magnitude of the far field hot gas ingestion is greatly reduced in comparison to the near field because of the exhaust jet flow mixing with the ambient air flow.

This paper will present results obtained at the compressor face of a 9.2 percent scale vectored thrust STOVL model in ground effects from Phases I and II. The STOVL model had a unique model support system. The model support system had four degrees of freedom; pitch, roll, yaw, and vertical height variation, heated high pressure air for nozzle flow, and a suction system exhaust for inlet flow. During Phase I testing the model support system was manually operated. However, Phase II testing had the model integrated support system (MISS) operated remotely from the control room. For the purpose of this report, only the height variation was used on the MISS. The pitch, roll, and yaw were set initially and kept constant thereafter. The hot gas ingestion results are shown for a headwind (freestream) velocity of 10 kn. A limited amount of data are presented with headwind velocities up to 90 kn, from Phase I testing. The near and far field sheet laser flow visualization are presented for the span and streamwise laser positions.

Facility, Model Configurations and Support System

The NASA Lewis 9- by 15-Foot Low Speed Wind Tunnel (LSWT) was used to develop the hot gas ingestion database. The 9- By 15-Foot LSWT, constructed within the return leg of the 8- By 6-Foot Supersonic Wind Tunnel (SWT), is shown schematically in Fig 2. Tunnel velocities from 8 to 23 kn were set by using the air dryer blowers and number 4 and 5 doors.

A schematic for the HGI model, MCAIR model 279-3C, is shown in Fig 3. The model consisted of five major subassemblies; the forward fuselage, center fuselage, aft fuselage, the wings, and canards. The forward fuselage contained the main inlet and a translating cowl auxiliary inlet which makes up the bifurcated inlet system. The inlet suction duct is part of the suction system and was used to create inlet (compressor face) flow. The center fuselage contained the nozzle system; high pressure hot air lines supplied hot air (1460 °R) to the model's four nozzles. Lift improvement devices (LIDs) would also be attached to the center fuselage.

The LIDs consist of longitudinal strakes, sidewalls, forward fence and aft fence (optional). The LIDs generally enclosed the forward and aft pair nozzles. The undersurface of the HGI model with the 0° forward nozzle splay configuration is shown in Fig 3.

The definition of the forward nozzle splay angle is shown in Fig 4(a). The splay angle is measured with reference to a vertical line through the nozzle centerline. A negative splay means the nozzles are in-board of the vertical line.

The nozzle vector thrust angle is shown in Fig 4(b). The nozzle vector angle for the data presented in this paper is 82° on the forward nozzles and 83.5° on the aft nozzles. The

model was capable of vectoring thrust from 0° (full aft) to 110° (slightly forward).

Model Installed in the 9-By 15-Foot Low Speed Wind Tunnel

A schematic of the installation of the 9.2 percent scale model and the supporting system in the 9-By 15-Foot Low Speed Wind Tunnel (LSWT) are shown in Fig 5. The supporting system includes a remotely controlled model integrated support system (MISS) that had four degrees of freedom (model height, yaw, pitch, and roll). Figure 6(a) shows the model and MISS installed in the 9- By 15-Foot LSWT. A ground plane was installed with static pressures, air temperature instrumentation and boundary-layer rakes. The ground plane had a sliding trap door. The trap door was open when the nozzle conditions were being set and closed to set up the steady state conditions during data recording. For hot gas ingestion testing the section of the trap door under the model was covered with flat pieces of shuttle tiles. The tiles were used so the structure of the trap door would not see the 1460 °R nozzle airflow temperature. When laser sheet testing was conducted the tiles were covered with a thin stainless steel sheet to prevent water, used for flow visualization, from damaging the tiles and trap door instrumentations. Figure 6(b), an aft view of the installation in the 9-By 15-Foot LSWT shows the ground plane ejector system which evacuated the hot exhaust gases from the vicinity of the model when the nozzle flow conditions were being set. The ejectors were automatically shut off when the trap door closed.

Two heaters were used for the 1460 °R nozzle airflow temperature. One heater supplied airflow for the front nozzles and the other heater supplied airflow for the aft nozzles. Each heater is capable of delivering 1100 °F process air at 5 lb/sec and 450 psig.

A copper metal vapor laser which will be described in LASER SHEET FLOW VISUALIZATION was used to generate the illumination system for the flow field. The laser and turn key control system are shown in Fig 7.

A schematic of the ground plane is shown in Fig 8. The ground plane was 336 in. long and 176 in. wide and was 18 in. off the wind tunnel floor. The trap door opening was 42 in. in the axial direction and 40.75 in. in the span direction. The trap door closed from a full open position in 0.5 sec.

A cross section view of the test section is show in Fig 9. The test section is normally lined with an acoustic treatment. For the hot gas ingestion tests, the floor treatment was removed and steel plates were installed as the tunnel floor. The ground plane system was attached to the steel floor. The lower part of the tunnel walls were removed so that the hot gases from the nozzles could flow out beyond the test section walls and mix with cooler air before entering the downstream diffuser section. A trap-door-scavenging system was located under the ground plane. When the nozzle pressure ratios are being set, the trap door is open, allowing the hot exhaust gases to exit the test section without heating the model, ground plane, and the local environment. When the trap door is closed, the lateral flow from the nozzle jets exit the test section through the sidewall bleed system (located on both the left and right sidewalls) and thereby preventing circulation of the tunnel and jet airflow.

Model and Ground Plane Instrumentations

The 9.2 percent scale model was instrumented along the underside of the fuselage, around the ramps and inlets (main and auxiliary), and also at the compressor face. The instrumentation consisted of static and total pressures, and protruding temperature probes (which measured the surface air temperature). The main objective of this paper is to present the results at the compressor face and results showing the flow field using a

sheet laser system. Hence, the model instrumentation other than the compressor face will be shown on each figure which is pertinent. Figure 10 shows the compressor face rake instrumentation: the location of each probe on the rake and the circumferential location. Each rake arm was made up of four total pressure and five total temperature measurements. One wall static pressure tap was located by each rake arm around the circumferential. Only steady state measurements were made during this test program.

The ground plane centerline instrumentation and the ground plane rakes are shown in Fig 11. The centerline instrumentation consisted of static pressures and flush mounted thermocouples (temperature taps) which were isolated from the plate surface so as to measure the ground plane air temperature. There were three double sided instrumented rakes and two single sided instrumented rakes. The double sided rakes measured the free-stream side flow and the flow coming from the nozzle jets (model side). The single sided rakes measured only the model side of the flow. There were two rake heights, 4.0 and 11.0 in. Each rake contained total pressure, total temperature, and static pressure measurements. Additional instrumentation was located on the trap door and other section of the ground plane.

The test section airflow velocity measuring system is shown in Fig 12. The anemometer was located on the test section ceiling near the entrance of the test section. The anemometer is capable of measuring velocities from 1 to 98 kn within ±0.6 kn. The hot gas ingestion testing was generally conducted between velocities of 8 and 23 kn.

Laser Sheet Flow Visualization

The flow field from the deflected thrust nozzles can be visualized by using a seeding agent in the nozzle airflow and intensifying the flow with a laser sheet. This laser sheet was produced using a 15 W copper vapor laser coupled with a fiber optic delivery system to take the laser beam to the test section. An optic head housing lenses was coupled to the other end of the fiber cable. The lenses produce a sheet of light that is approximately 18 in. high and 0.125 in. wide at the centerline of the model. The optic head was mounted on a single axis traverse to allow remote control of the light sheet positioning and quick repositioning in the tunnel. The laser operates in the 510.6 and 578.2 nm wavelength.

To view the flow field an array of video and still cameras were used. As many as five color video cameras were mounted at different tunnel stations in order to get the best views of the flow field and obtain maximum light levels. The video data was recorded on 0.75 in. Umatic format and 0.5 in. VHS tape. Still photographs were taken using a combination of remotely controlled 70 and 35 mm cameras.

Data Acquisition

The data system used for hot gas ingestion testing in the 9-By 15-Foot LSWT was NASA Lewis central data acquisition system. The data system reads 512 channels of pressures, 330 analog inputs of which 440 are thermocouples, does all calculations, and displays the results once per second at the test facility.

Dynamic data measurement was taken with an array of microphones for far field noise and fluctuating pressures on the fuselage, canard, and wing using water-cooled pressure transducers able to withstand the 1460 °R exhaust nozzle airflow. This data are not a part of this paper.

Results and Discussion

Phase I

The basic objectives of Phase I were to develop and demonstrate STOVL HGI control techniques and establish a hot gas ingestion database for exhaust nozzles temperature up to 960 °R; and establish an air flow visualization

database using white light as the illumination source.

Phase I testing was conducted up to an exhaust nozzle temperature of 960 °R and over a headwind velocity ranging from 8 to 90 kn. The effect of both model main landing gear height (model height) above the ground plane and headwind velocity on the compressor face temperature rise are presented for the clean and LIDs configurations. The forward nozzle splay angles for these configuration are -6° and 18°. The design nozzle pressure ratio is 3.06 for the forward nozzles and 3.16 for the aft nozzles. The design landing headwind velocity is 10 kn. The white light flow visualization is shown for a 23 kn headwind velocity and design nozzle pressure ratios.

Phase II

The basic objectives of Phase II were to extend the database for model 279-3C to 1460 °R; establish an acoustic and structural acoustic database at exhaust nozzle temperature up to a 1460 °R; obtain data for temperature scaling; and establish an air flow visualization database using a high energy fiber optic laser sheet illumination system.

Phase II was conducted with an exhaust temperature up to 1460 °R and over a headwind velocity ranging from 10 to 23 kn. A sheet laser system was used as the illumination source for the flow visualization test in Phase II. The nozzle pressure ratio and inlet throat Mach number were the same for both phases.

The test results obtained during HGI Phase II are presented for the 0° splay forward nozzles configuration at a main landing gear height (model height) of 0.20 in. above the ground plane. The hot gas ingestion data are presented for a nozzle design pressure ratio of 3.02 on the forward nozzles and 3.16 on the aft nozzles. The compressor face Mach number was 0.40; pitch angle, 6.5°; and headwind velocity, 10 kn.

The laser flow visualization data are shown for headwind velocities of 10 kn; nozzle pressure ratios of 3.06, forward nozzles; and 3.16, aft nozzles. Data are also shown for a headwind velocity 23 kn and nozzles pressure ratio of 1.74.

The test results are presented in a sequence which parallels the overall test approach:

HGI Phase I:
- Clean Model Results
- Lift Improvement Devices (LIDs) Comparison Results

HGI Phase II:
- Zero degrees forward nozzle splay angle
- Clean and LIDs Comparison Results

Clean Model Test Results

The clean model was tested to obtain baseline data for comparison with LIDs configurations. The key test variables for this baseline testing is model height, which is the height the main landing gear is above the ground plane, headwind, and forward nozzle splay angle.

Height Effect The compressor face temperature rise as a function of model height above the ground plane for two forward nozzle splay angles -6° (baseline) and 18°, is shown in Fig 13. With the initial model height decrease into ground effects the change of compressor face temperature rise is small due to changes only in far field HGI. With further descent, the model eventually reaches the height at which the fountain caused by the interaction of the nozzle jets forms and near field HGI begins. The compressor face temperature rise increases rapidly below this height because the fountain formation point (transition to "in ground effects") is indicated as a distinct change in slope of the compressor face temperature rise curve. This slope change is seen in the -6° forward nozzle splay data at 0.6 in. model height, and in the 18° splay data at

4.7 in. model height. The formation height and magnitude of the near field HGI can therefore be altered through changes in forward nozzle splay angle. Knowledge of such HGI changes with height are essential for accurate prediction of STOVL aircraft vertical landing performance.

Headwind Effect The effect of headwind on the baseline HGI levels at low model height is shown in Fig 14. From 8 to 70 kn headwind, the compressor face temperature rise increases because the headwind moves the ground flow separation point closer to the model and the far field HGI mixes less with ambient air. At 70 kn, the compressor face temperature reaches a maximum because the ground flow separation point is coincident with the inlet and minimal mixing occurs prior to ingestion. Further increases in headwind decrease the compressor face temperature rise because the separation point moves behind the inlet. Headwind velocity therefore affects HGI levels by changing the ground flow separation point, and the far field cloud mixing characteristics and height. The results show that headwind effects increase the compressor face temperature rise at low model heights for the baseline range of headwind (8 to 23 kn) and therefore, should be included in all STOVL aircraft HGI assessments.

LIDs Test Result

The selection of a preferred LIDs configuration must take into consideration not only HGI, but jet induced lift, and airframe integration. Since jet induced lift testing was not conducted for the LIDs configuration, a preliminary selection was made based on MCAIR V/STOL experience. This experience indicated that incorporation of a forward fence and longitudinal strakes would provide acceptable jet induced lift and that the addition of an aft fence would provide little benefit. Also, increased LIDs depth would increase jet induced lift. With respect to airframe integration, the largest feasible LIDS were used.

Height Effect. Compressor face temperature rise as a function of height for both the clean and preferred LIDs configuration is shown in Fig 15(a) for a forward nozzle splay angle of -6°. The LIDs capture the fountain upwash and redirect it downward away from the inlets. This results in substantial decreases in HGI for heights where a fountain has formed (below 0.6 in. for -6° splay. LIDs also have a positive effect when the forward nozzle splay is 18° (Fig 15(b)). There is a significant reduction in HGI over the heights where there is a fountain upwash (below 4.7 in.). The LIDs are less effective for reducing HGI with this nozzle splay because the impact area of the fountain on the fuselage undersurface extends beyond the perimeter of the LIDs and the fountain is not captured as well as with the -6° nozzle splay.

Headwind Effect. The effect of LIDs on compressor face temperature rise with variations in headwind is shown in Fig 16. Only the far field HGI component of compressor face temperature rise is shown since the near field compressor face temperature rise is generally constant with headwind velocity for a fixed model height above the ground plane. The far field component is calculated from the total compressor face temperature rise by subtracting the rise associated with the near field HGI. The near field temperature rise can be determined by extrapolating the total compressor face temperature rise to the zero headwind condition where there is no far field HGI. Compressor face temperature rises obtained with LIDs as a function of headwind had a lower maximum far field compressor face temperature rise which occurs at a higher headwind velocity, compared to the clean configuration. This results from the downwash flow off the LIDs forward fence merging with, and strengthening, the ground jet flow in front of the aircraft. This pushes the far field separation point away from the aircraft so the far field compressor face temperature rise decreases. This is a significant

result since the LIDs were previously believed to control only the near field HGI. These results were also verified by the flow visualization data.

Inlet Temperature Distortion. The main source of inlet temperature distortion in ground effect is the near field HGI. In the clean configuration, ingestion of near field HGI causes inlet temperature distortion in the form of a localized high temperature region at the bottom of the engine face (left side of Fig 17).

LIDs were found to be very effective in reducing inlet temperature distortion. They minimize near field HGI by inhibiting the forward movement of the upwash along the fuselage. When LIDs were added, the temperature distortion at the engine face was significantly reduced, (right side of Fig 17), due to elimination of the near field HGI. This causes the far field HGI to dominate and since it is better mixed with the ambient air, engine face temperature distortion is essentially eliminated.

HGI: Phase II Test Results

The test results presented in this section are for a 0° splay forward nozzles configuration at a main landing gear height (model height) Of 0.20 in. above the ground plane. These results are typical for the 0° splay configuration at the 23 kn condition.

The compressor face temperature as a function of the model height (main landing gear height above the ground plane) above the ground plane. is shown in Fig 18(a) for the clean configuration and two nozzle temperatures, 960 and 1210 °R. As the model descends toward the ground the change in the compressor face temperature rise is small and may be indicative of the far field temperature. As the model descends into ground effects the near field effects are set up, the fountain forms under the model, hence the compressor face temperature rise increases rapidly. In general, hot gas ingestion occurs where the change in the compressor face temperature rise begin increasing rapidly. The data indicate that the magnitude of the nozzle exhaust temperature influences the level of the compressor face temperature rise when the model is in ground effects. When LIDs are added to the underside of the fuselage (Fig 18(b)), a substantial reduction occurs in the compressor face temperature rise in comparison to the clean configuration. The magnitude of the LIDs compressor temperature rise is an indication of the effectiveness of the LIDs. The LIDs data tend to show ground effects at about 2 in. above the ground plane.

The effect of nozzle exhaust temperature on the compressor face parameters at nozzle pressure ratios of 3.02 for the forward nozzles and 3.16 for the aft nozzles is presented in Fig 19. The data are shown as bar graphs for simplicity. Figure 19(a) shows the clean configuration with nozzle exhaust temperatures of 960 and 1160 °R. In general, an increase in the temperature resulted in an increase in all the compressor face parameters except the for total pressure recovery. The total pressure recovery was reduced very slightly. However, the total pressure distortion was about one percent higher at the higher temperature. The largest impact occurred on the temperature parameters, such as the temperature distortion, increasing by five percentage points, and the compressor face temperature rise, increasing by 35 °R. Figure 19(b) contains the result with LIDs on the undersurface of the model. The LIDs are used to capture the fountain as the model descends into ground effects, hence improving the jet induced lift. The LIDs also serve to deflect the hot gas away from the inlet/fuselage region, thereby reducing the hot gas ingestion when in ground effects. The results shown in Fig 19(b) indicate that the LIDs were a significant factor in reducing the effect of HGI caused by ground effects. For example, the compressor face temperature rise was only 29 °R with LIDs and 145 °R in the clean configuration at a nozzle exhaust temperature of 1160 °R. Other

compressor face parameters were also generally better with LIDs than with the clean configuration. The total pressure recovery was 0.99 with LIDs and 0.97 without LIDs.

Since the upwash fountain will interact with the undersurface of the fuselage, the temperature distribution under the model will often show interesting distributions. Figure 20, shows the surface air temperature along the undersurface of the fuselage from the aft landing gear to the main inlet station for two nozzle exhaust temperatures. The clean configuration (Fig 20(a)) always had higher surface air temperatures over the entire length of the fuselage. The LIDs configuration (Fig 20(b)) had about the same level of surface air temperature as the clean configuration downstream of the LIDs, station 27.50 in. However, upstream of the LIDs, from station 27.50 through station 10.80 in., the surface air temperature was substantially reduced.

The ground plane distribution of the temperature and pressure profiles are shown in Fig 21(a) for the clean configuration and in Fig 21(b) for the LIDs configuration. In general, the temperature and pressure environments reflect the conditions encountered by the compressor face, due to near field and far field HGI. The ground plane centerline distance is measured from the mid-point between the forward and aft nozzle. The near field temperature and pressure are reflected in the ground plane centerline distances, -15 and 11 in. In this region all of the pressure changes take place and much of the temperature rise and decay occurs. The pressure field reflects that this region is under a suckdown (negative) pressure (Fig 21). The surface air temperature along the ground plane remains attached through the end of the ground plane, at a centerline distance of 139 in. Shown in Fig 21 is the headwind temperature which is below the temperature distribution. This indicates the flow was attached although the ground jet had to travel from the midpoint between the forward and aft nozzles. Video data taken during this test also confirmed this result. As seen in Fig 21(b), the temperature distribution with LIDs tend to dropoff at a higher rate than it does with the clean configuration, at a ground plane centerline distance of 14.00 in.

Figure 22(a) shows a typical three-dimensional surface contour plot of the trap door. Typical ground plane three-dimensional surface contour plot is presented in Fig 22(b) for the clean configuration at headwind velocity of 10 kn and at design condition. In general these figures indicate the lateral and the axial decay of the temperature from the maximum source, the exhaust nozzles. The hottest temperature region on the trap door is located under the aft and forward nozzles. The highest temperature on the ground plane occurred at the edge closest to the trap door. These plots represent only one side of the model for the forward and aft nozzles.

Flow Visualization

During the Phase I flow visualization testing white light was used as the illuminating source. A typical far field separation is shown in Fig 23 using water as the seeding. The tufts on the ground plane pointing toward the model are under the influence of the headwind velocity and upstream of the far field separation zone. The tufts pointing away from the model are under the influence of the nozzle flow and are downstream of the separation zone. The tufts in the separation zone often have a 90° to 180° movement (pointing at the model to an away position). The influence of the ground jet was confined laterally by the headwind velocity, due to the lateral velocity decay. The lateral confinement of the ground jet can be seem at the top of Fig 23. The tufts in the upper region are pointing downstream.

Characteristics typical of the near field hot gas ingestion problem are shown in Fig 24. Shown is a three-quarter view of the clean configuration with a -6° forward nozzle splay angle. When the ground jet flow from two nozzles meet, a fountain is

formed. If there are more than two jets, fountain is formed between each pair and a central fountain is formed when the flow from all four nozzles meet. Between the forward and aft nozzles is a stagnation line. The central fountain can also be seen in the aft region under the model.

During the hot gas ingestion testing of Phase II, a flow visualization test was also conducted using a sheet laser as the illuminating source. The laser optic package could be mounted such that the flow field in any of the three planes could be viewed. The optic package was mounted on a traversing mechanism which allowed detail observations of several stations over a range of 48 in.

Figure 25 shows the span-wise sheet of the flow field under the model. Figure 25(a) shows the laser sheet at the centerline of the forward nozzles which are at a 0° splay angle. The nozzles have a built-in splay of 24°, hence zero degrees mechanical splay angle produce an 18° internal aerodynamic splay angle. The upwash fountain can be seen as the bright spot under the lower fuselage. This is the upwash fountain caused by the two forward nozzles and the source of the near field hot gas ingestion. The flow field near the auxiliary inlets section is shown in Fig 25(b). The upwash fountain also exists at this station and tends to interact with the underside of the fuselage. At the low heights above the ground plane the ground effects tend to be confined to the region surrounding the plan form of the model. Figure 25(c), shows the flow field at the main inlet station. The lower part of the main inlet and the underside of the fuselage both indicate flow field interaction. The illuminated flow field shown here are the source of hot gas ingestion. This influence of the ground plane show up in the lower section of the compressor face as a region of elevated temperature.

In order to observe both the near and far field environment, it is necessary that the laser sheet be in the streamwise direction. Figure 26 shows such a view. The upwash fountain between the forward nozzles and also the far field ground jet can be seen. The far field separation, in this case, is not clearly defined. Also the far field ground jet separation tends to be very turbulent.

During the flow visualization testing, an image enhancement system was also used. Figure 27(a) shows the gray level from the video. The false color enhancement is shown in Fig 27(b). The flow fields are shown for a 23 kn headwind velocity, nozzle pressure ratio of 1.70, model main gear height above the ground plane of 12 in.; pitch angle, 6.5°; and inlet Mach number of 0.40. The color enhancement can be done in real time during the testing. The change in intensity of the concentration of the seeding agents can be seen during what appears to be a steady state condition.

Concluding Remarks

The basic objectives of Phase I, to develop and demonstrate STOVL HGI control techniques and Phase II, to extend the database for model 279-3C to 1460 °R; establish an acoustic and structural acoustic database at exhaust nozzle temperature up to a 1460 °R; obtain data for temperature scaling; and establish an air flow visualization database using a high energy fiber optic laser sheet illumination system, were successfully met. Significant reductions in HGI were obtained through the combined use of LIDs and forward nozzle splay angle.

Both phases of the test program produced an extensive database for indepth understanding of HGI phenomena. The data will be used to improve HGI empirical prediction techniques for screening future STOVL aircraft concepts during preliminary design.

The copper vapor laser sheet illumination system provided insight into the vectored thrust flow field when the model was in and out of

ground effects. In general, the characteristics of the fountain is a function the forward nozzles splay angle and the height above the ground plane.

The use of false color image enhancement system reveal the dynamic of the central core located under the fuselage at low height above the ground. The image enhancement system was useful in depicting both the far and near field.

The NASA Lewis HGI test facility was validated as an excellent facility for accurately testing STOVL HGI. This validation established NASA Lewis as a national facility for STOVL HGI testing.

References

1. Johns, A.L., Flood, J.D., Strock, T.W., and Amuedo, K.C., 1988, "Hot Gas Ingestion Testing of an Advanced STOVL Concept in the NASA Lewis 9- by 15-Foot Low Speed Wind Tunnel With Flow Visualization," AIAA-88-3025, NASA TM-100952.

2. Johns, A.L., Neiner, G., Flood, J.D., Amuedo, K.C., and Strock, T.W., "Engine Inlet Distortion in a 9.2 Percent Scale Vectored Thrust STOVL Model in Ground Effect," AIAA-89-2910, NASA TM-102358.

3. Amuedo, K.C., Williams, B.R., Flood, J.D., and Johns, A.L., "STOVL Hot Gas Ingestion Control Technology," ASME Paper 89-GT-323, June 1989.

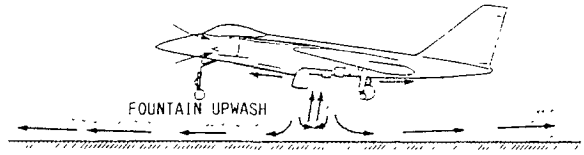

NEAR FIELD HOT GAS INGESTION DUE TO FOUNTAIN UPWASH

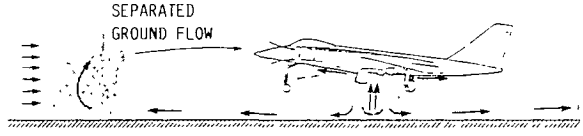

FAR FIELD HOT GAS INGESTION DUE TO SEPARATED GROUND FLOW

FIGURE 1. - SOURCES OF HOT GAS INGESTION.

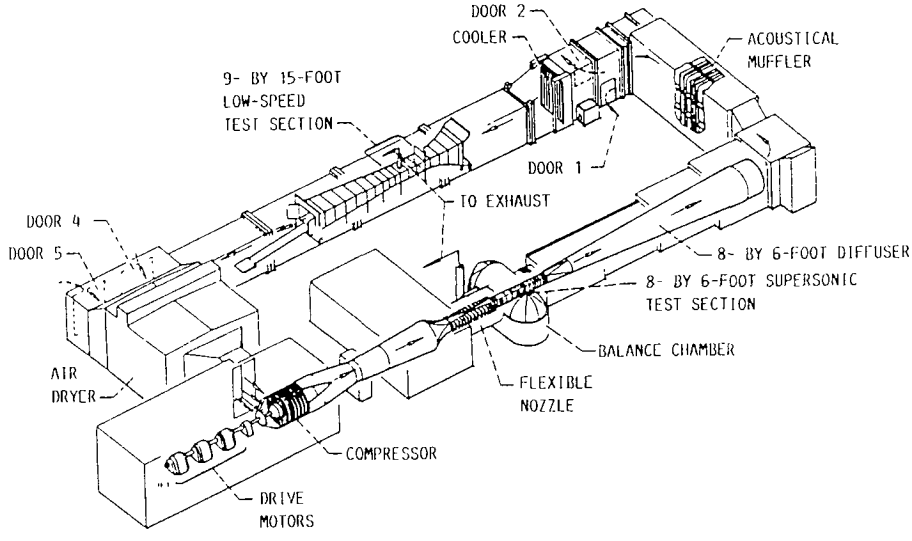

FIGURE 2. - AN ILLUSTRATION OF THE 9- BY 15-FOOT LOW-SPEED WIND TUNNEL AND THE 8- BY 6-FOOT SUPERSONIC WIND TUNNEL

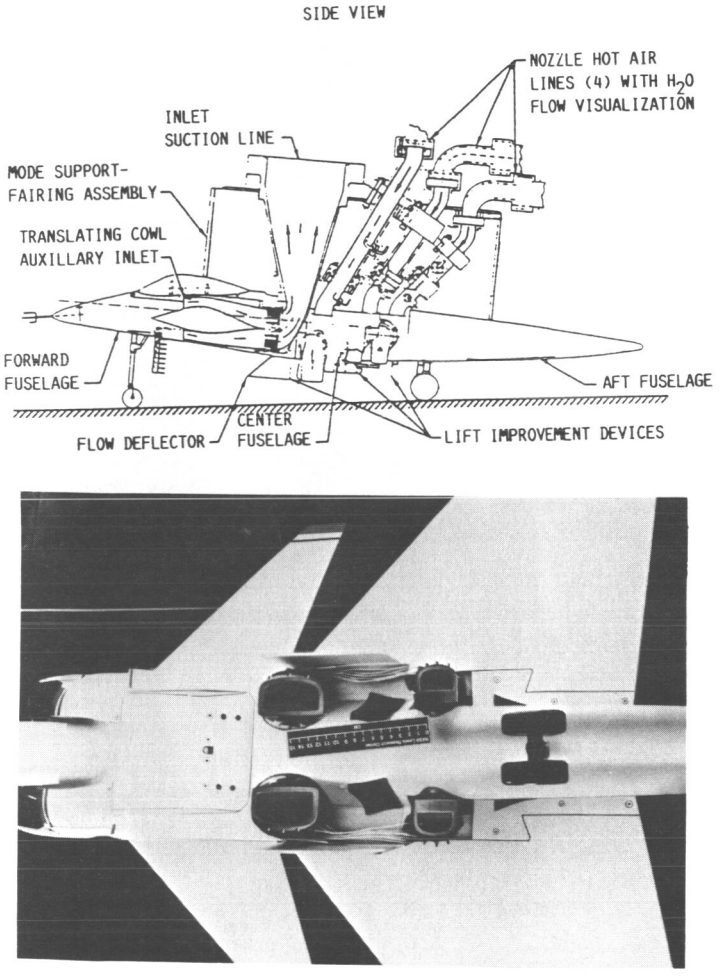

FIGURE 3. - SCHEMATIC AND UNDERSURFACE OF MODEL 279-3C.

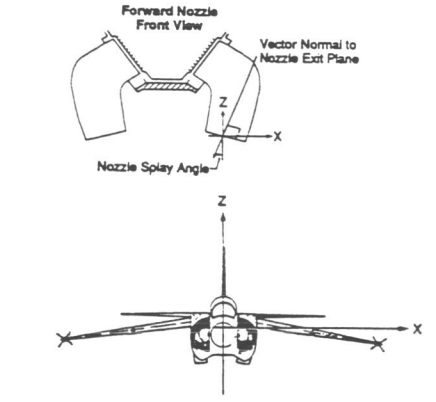

(a) NOZZLE SPLAY ANGLE.

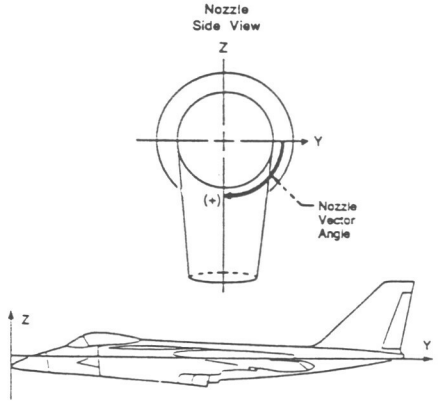

(b) NOZZLE VECTOR ANGLE.

FIGURE 4. - DEFINITION OF FORWARD NOZZLES SPLAY AND VECTOR ANGLES.

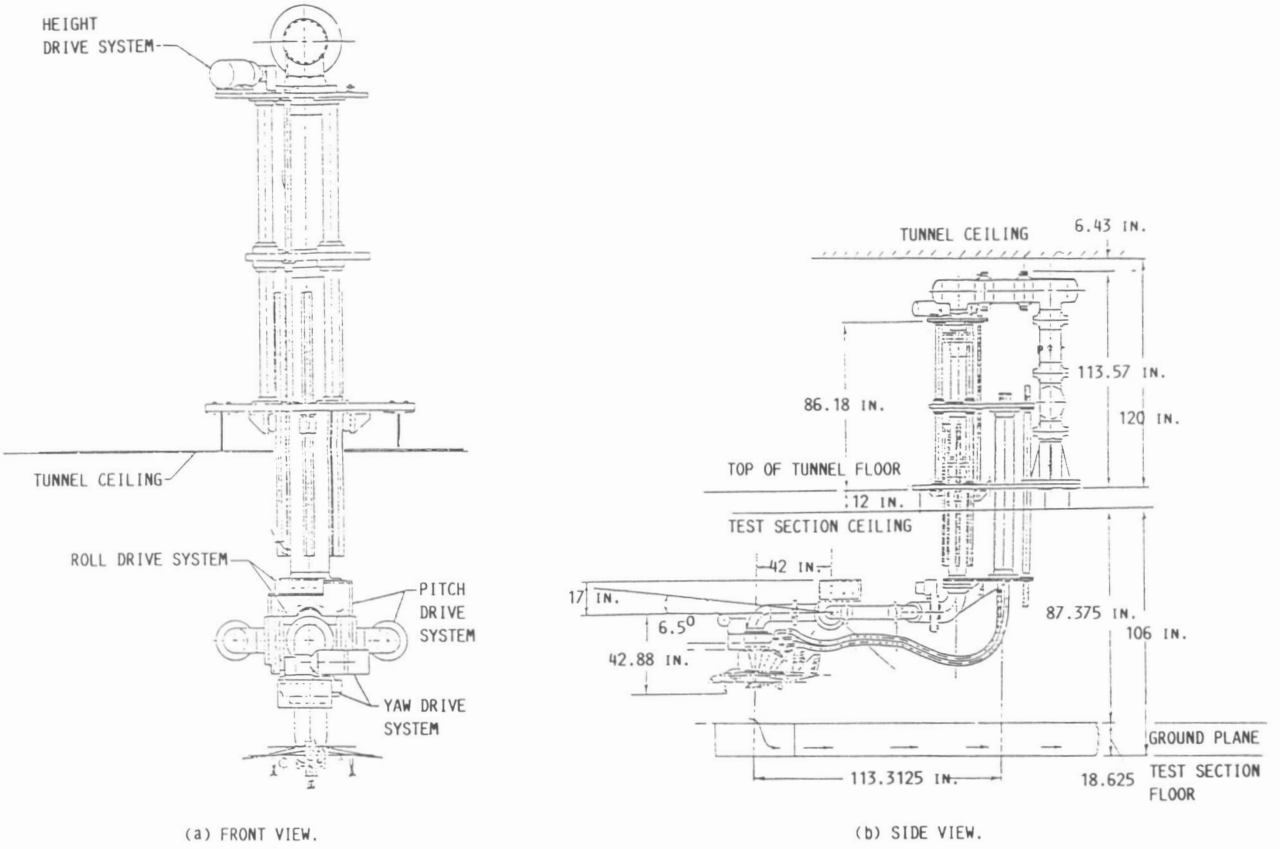

(a) FRONT VIEW.

(b) SIDE VIEW.

FIGURE 5. - MODEL INTEGRATED SUPPORT SYSTEM.

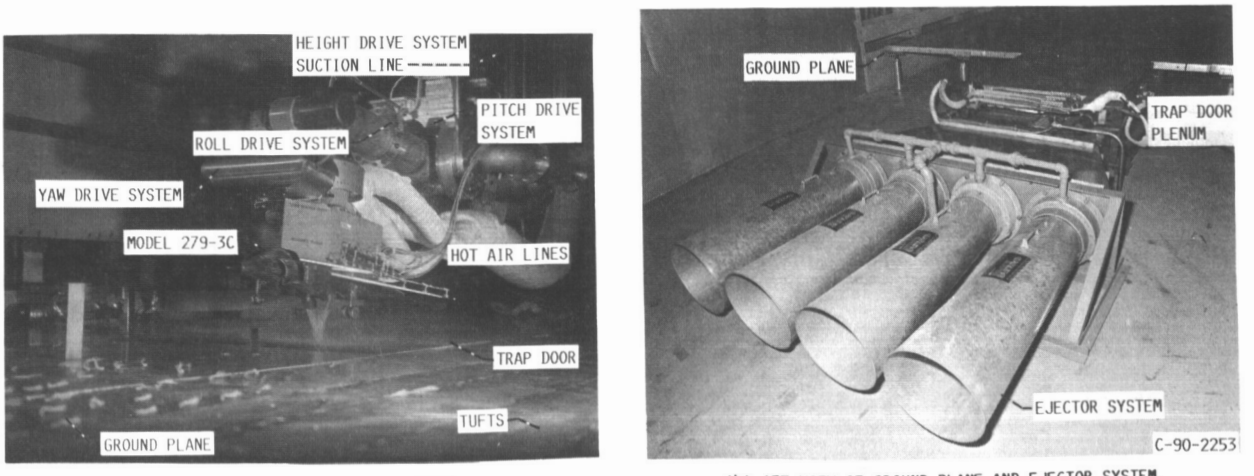

(a) MODEL AND "MISS" INSTALLATION.

(b) AFT VIEW OF GROUND PLANE AND EJECTOR SYSTEM.

FIGURE 6. - MODEL AND "MISS" INSTALLED IN THE 9- BY 15-FOOT LOW SPEED WIND TUNNEL.

ORIGINAL PAGE
BLACK AND WHITE PHOTOGRAPH

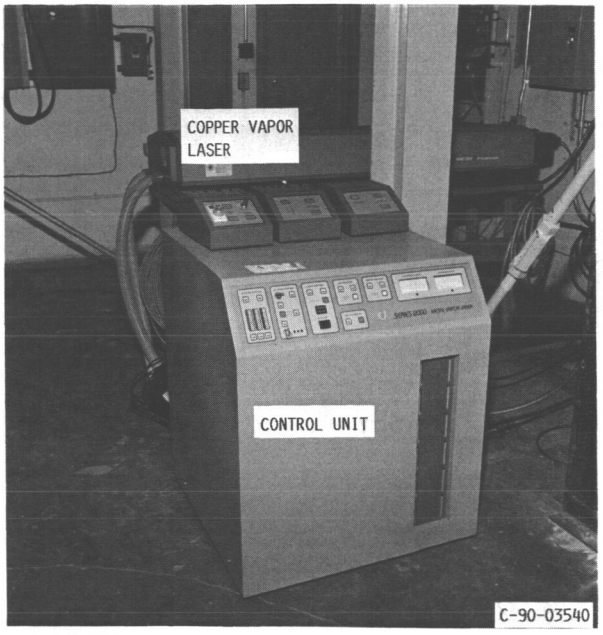

FIGURE 7. - COPPER VAPOR LASER AND CONTROL SYSTEM.

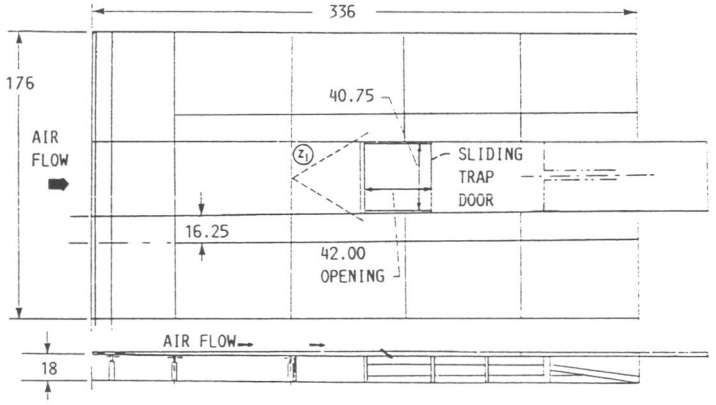

FIGURE 8. - SCHEMATIC OF THE GROUND PLANE. (DIMENSIONS IN INCHES).

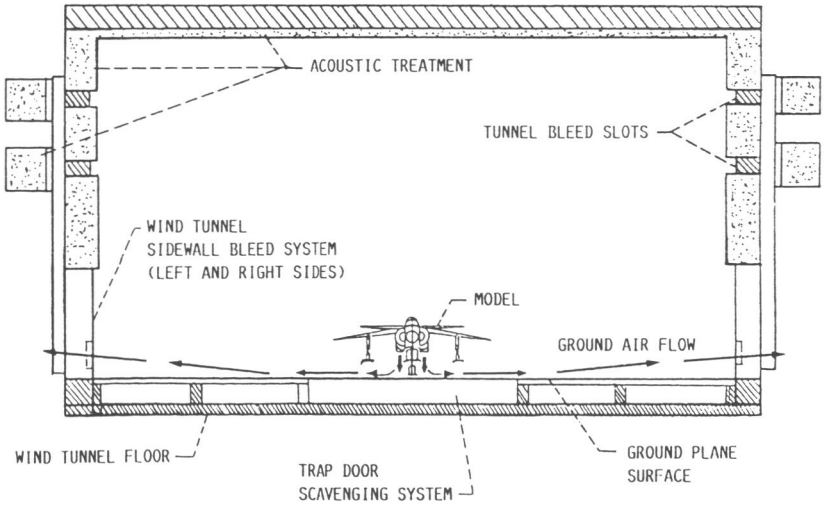

FIGURE 9. - CROSS SECTION OF THE TEST SECTION SHOWING THE SIDEWALLS BLEED AND TRAP DOOR SCAVENGING SYSTEMS.

LEG IDENTIFICATION			LEG IDENTIFICATION		
NUMBER	ANGLE, DEG	RADIUS, R, IN.	NUMBER	ANGLE, DEG	RADIUS, R, IN.
1	66.50		2	21.53	
4	293.50		3	338.47	
5	246.50		6	201.53	
8	113.50		7	158.47	
TOTAL TEMPERATURE		0.624	TOTAL TEMPERATURE		0.646
PRESSURE		0.698	PRESSURE		0.722
TEMPERATURE		1 081	TEMPERATURE		1.119
PRESSURE		1.209	PRESSURE		1 251
TEMPERATURE		1 396	TEMPERATURE		1 444
PRESSURE		1.560	PRESSURE		1.615
TEMPERATURE		1.651	TEMPERATURE		1.709
PRESSURE		1.810	PRESSURE		1.875
TEMPERATURE		1.872	TEMPERATURE		1.938
STATIC PRESSURE		2.038	STATIC PRESSURE		2.038

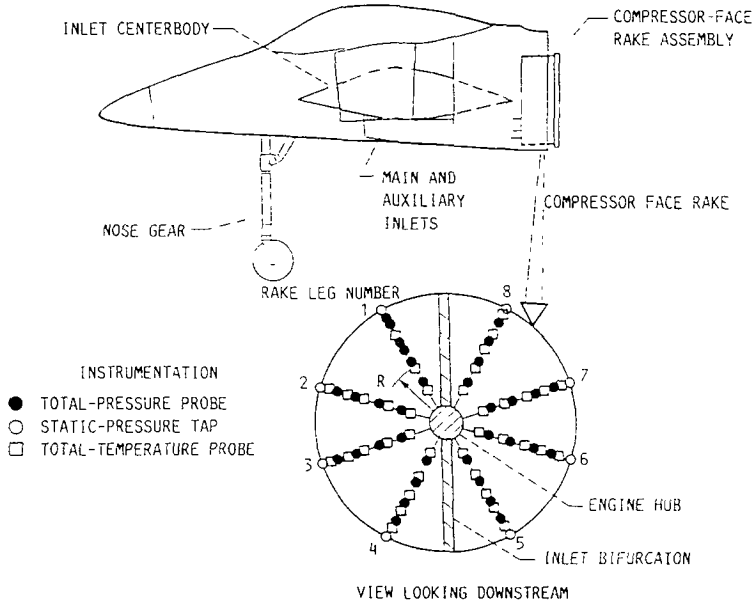

FIGURE 10. - COMPRESSOR FACE RAKE INSTRUMENTATION

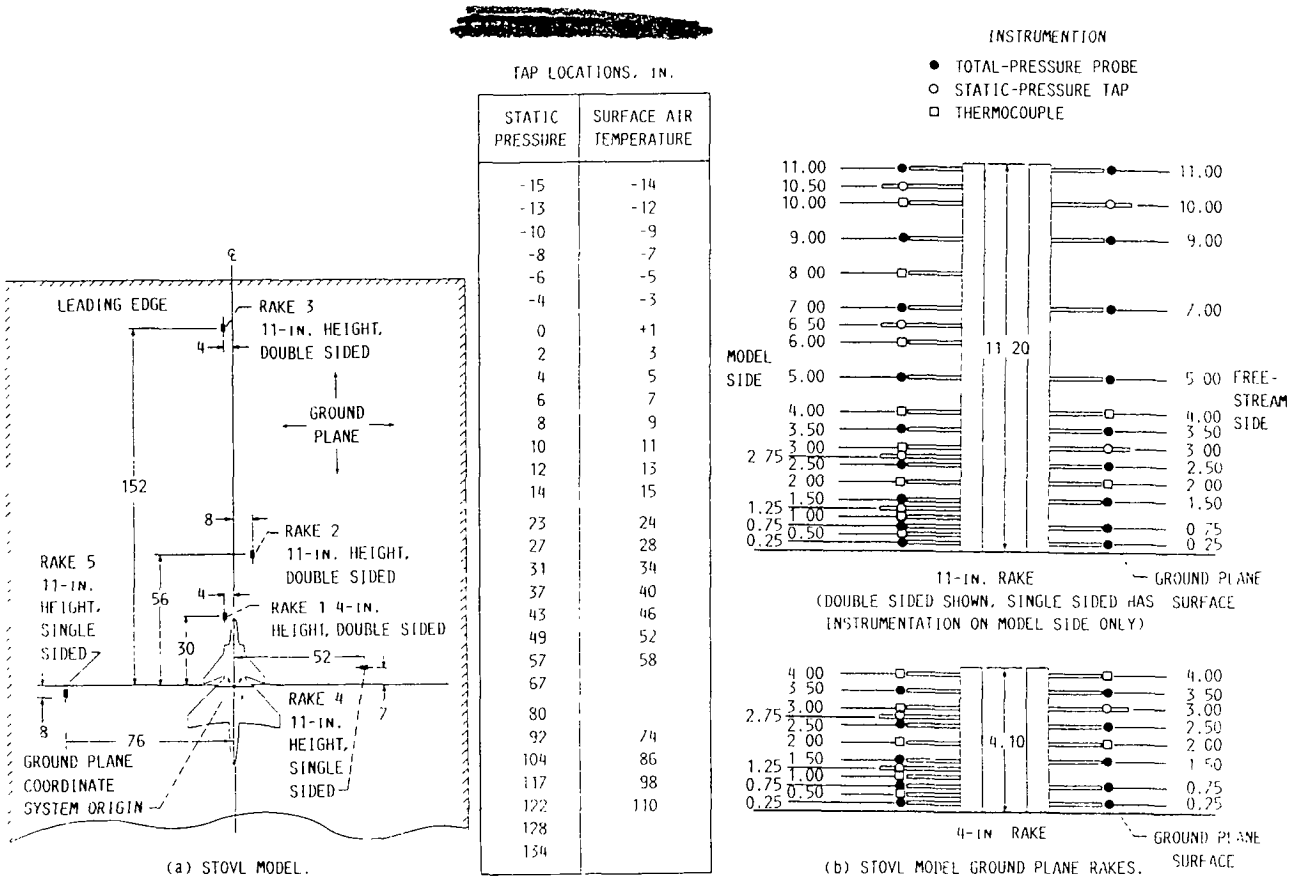

FIGURE 11. - GROUND PLANE INSTRUMENTATION, DIMENSIONS IN INCHES.

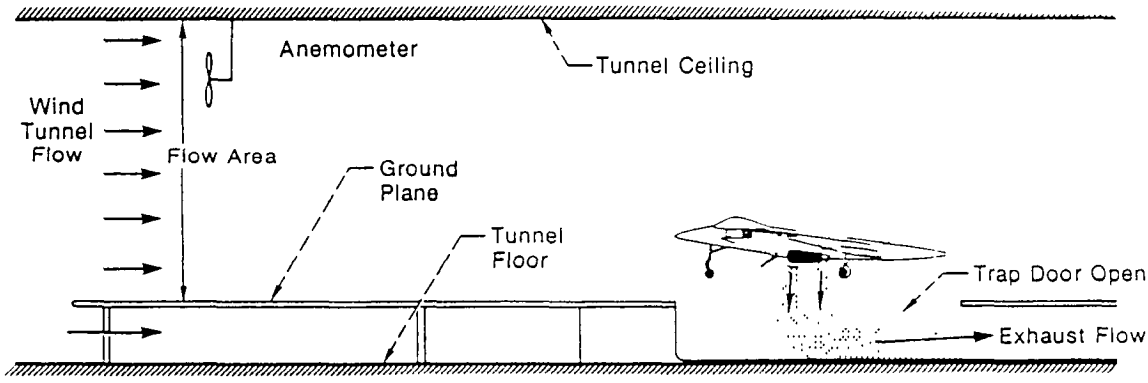

FIGURE 12. - TEST SECTION AIRFLOW VELOCITY MEASURING SYSTEM.

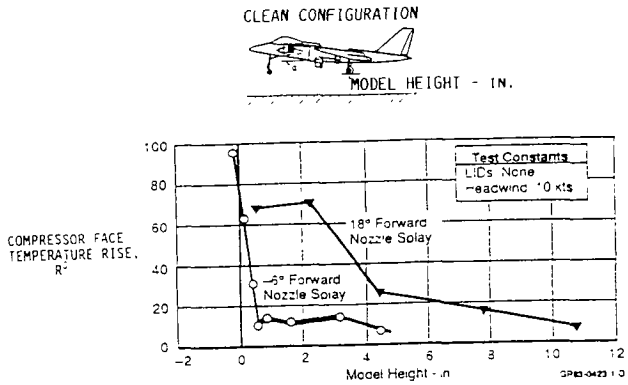

FIGURE 13. - HEIGHT EFFECT ON COMPRESSOR FACE TEMPERATURE RISE.

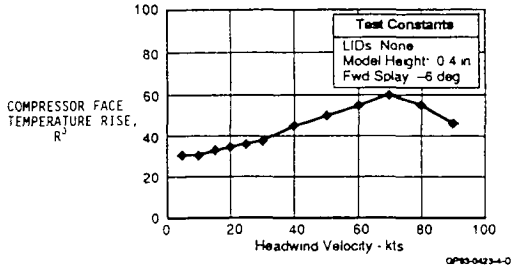

FIGURE 14. - HEADWIND EFFECT ON COMPRESSOR FACE TEMPERATURE RISE.

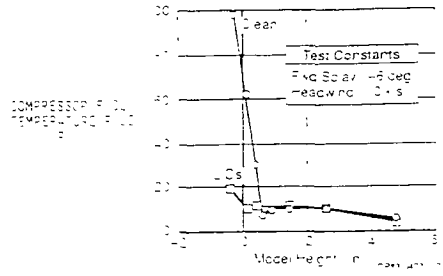

(a) -6° FORWARD NOZZLE SPLAY CONFIGURATION

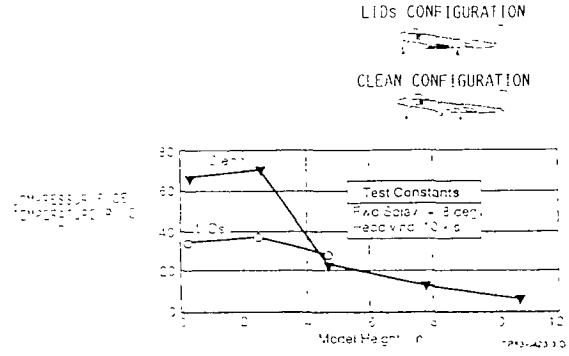

(b) 18° FORWARD NOZZLE SPLAY CONFIGURATION.

FIGURE 15. - EFFECT OF LIDs AS FUNCTION OF HEIGHT

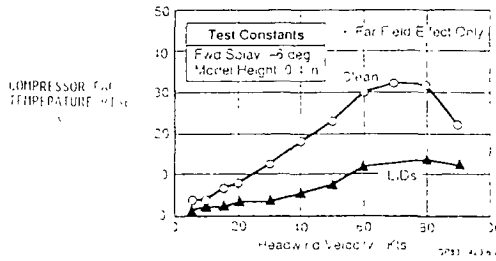

FIGURE 16 - EFFECT OF LIDs AS FUNCTION OF HEADWIND VELOCITY.

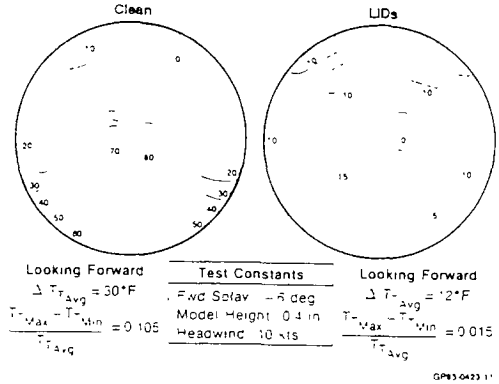

FIGURE 17 - ENGINE FACE TEMPERATURE RISE CONTOUR PLOTS

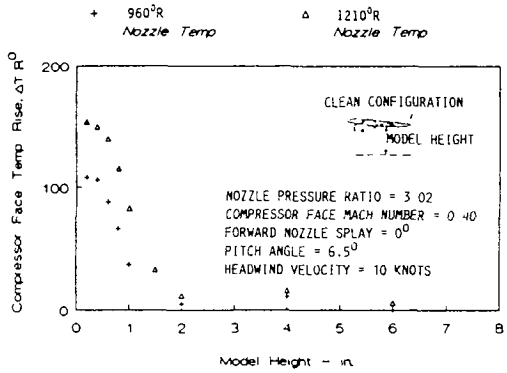

(a) CLEAN HEIGHT EFFECT ON INLET TEMPERATURE RISE.

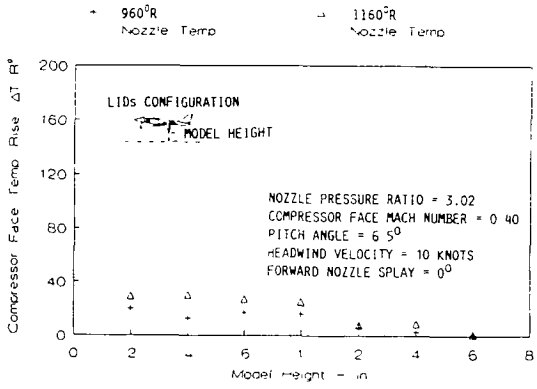

(b) LIDs HEIGHT EFFECT ON COMPRESSOR TEMPERATURE RISE.

FIGURE 18. - EFFECT OF THE MAIN LANDING GEAR HEIGHT ABOVE THE GROUND PLANE ON THE COMPRESSOR FACE TEMPERATURE RISE.

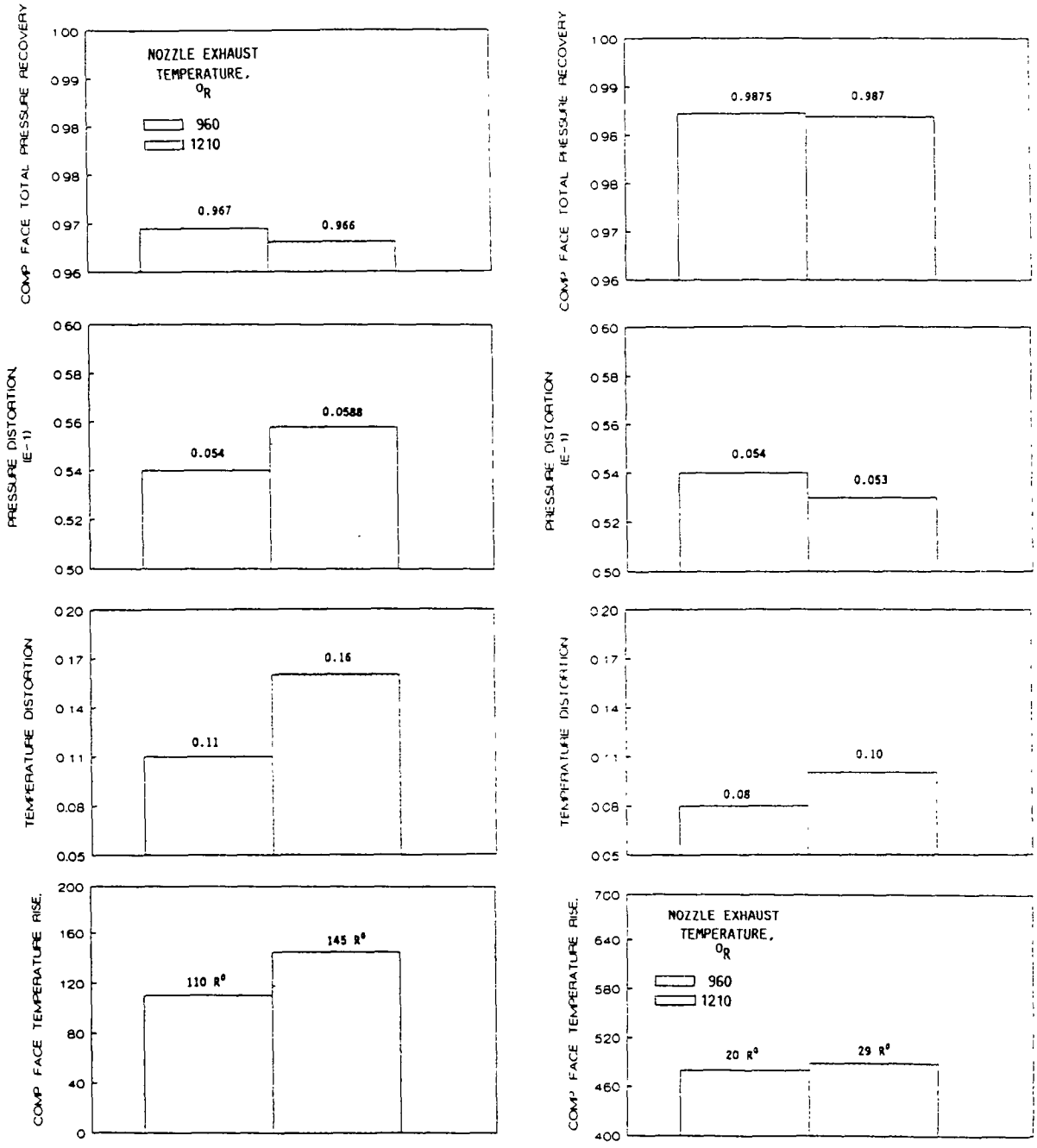

(a) CLEAN COMPRESSOR FACE PARAMETERS.

(b) LIDs COMPRESSOR FACE PARAMETERS.

FIGURE 19. - EFFECT OF NOZZLE EXHAUST TEMPERATURE ON THE COMPRESSOR FACE PARAMETERS AT NOZZLE PRESSURE RATIOS: FORWARD NOZZLES, 3.02; AFT NOZZLES, 3.16; COMPRESSOR FACE MACH NUMBER, 0.40; PITCH ANGLE, 6.5°; HEADWIND VELOCITY, 10 KNOTS.

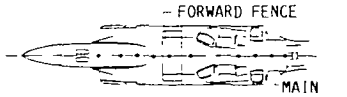

UNDERSURFACE OF MODEL 279-3C

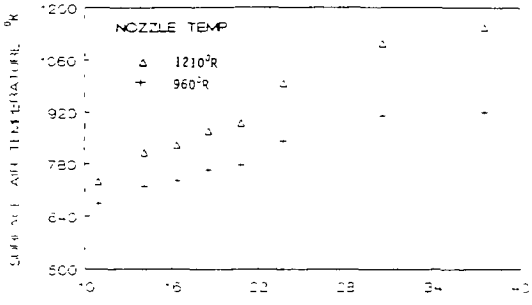

(a) CLEAN CONFIGURATION ZERO DEGREES, FORWARD NOZZLE SPLAY.

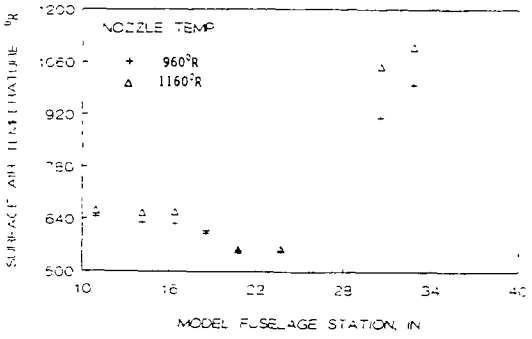

(b) LIDs CONFIGURATION ZERO DEGREES, FORWARD NOZZLE SPLAY

FIGURE 20 - FUSELAGE UNDERSURFACE AIR TEMPERATURE DISTRIBUTION AT 10 KNOTS AND NOZZLE PRESSURE RATIOS: FORWARD NOZZLES, 3 02; AFT NOZZLES, 3.16, COMPRESSOR FACE MACH NUMBER, 0 40; PITCH ANGLE, 6.5°.

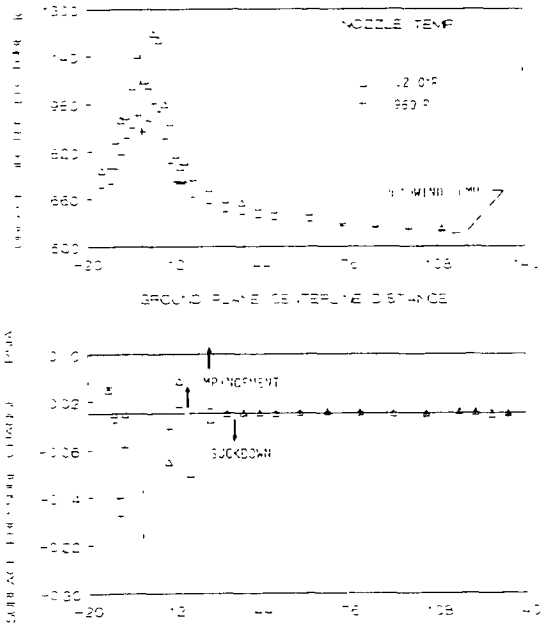

(a) CLEAN CONFIGURATION ZERO DEGREES, FORWARD NOZZLE SPLAY.

FIGURE 21. - GROUND PLANE CENTERLINE TEMPERATURE AND PRESSURE DISTRIBUTIONS AT 10 KNOTS AND NOZZLE PRESSURE RATIOS. FORWARD NOZZLES, 3.02, AFT NOZZLES, 3 16; COMPRESSOR FACE MACH NUMBER, 0.40; PITCH ANGLE, 6.5°

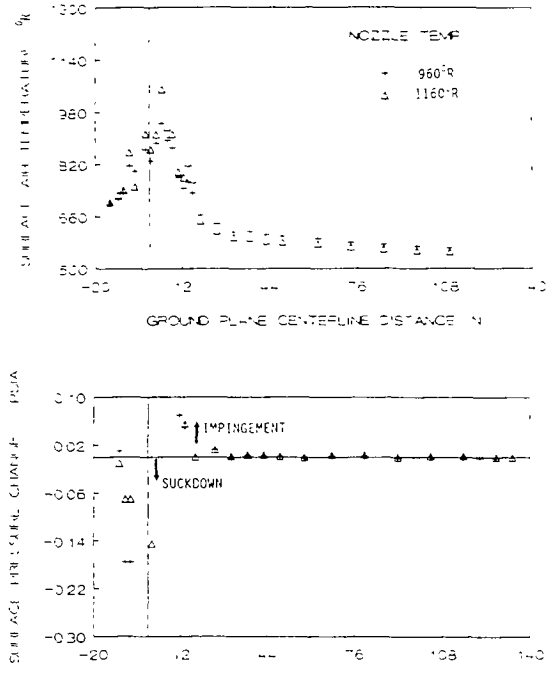

(b) LIDs CONFIGURATION ZERO DEGREES, FORWARD NOZZLE SPLAY.

FIGURE 21. - CONCLUDED

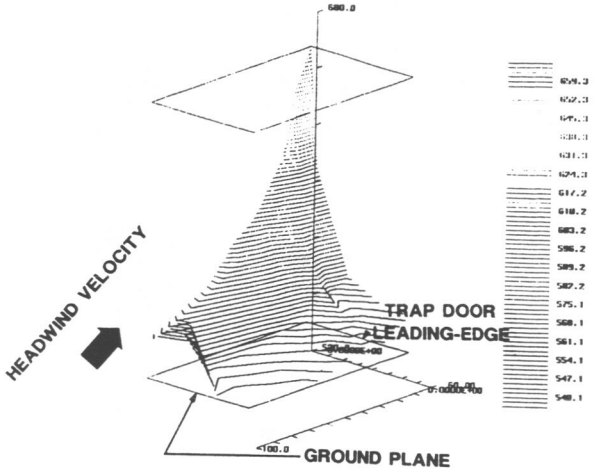

(b) GROUND PLANE.

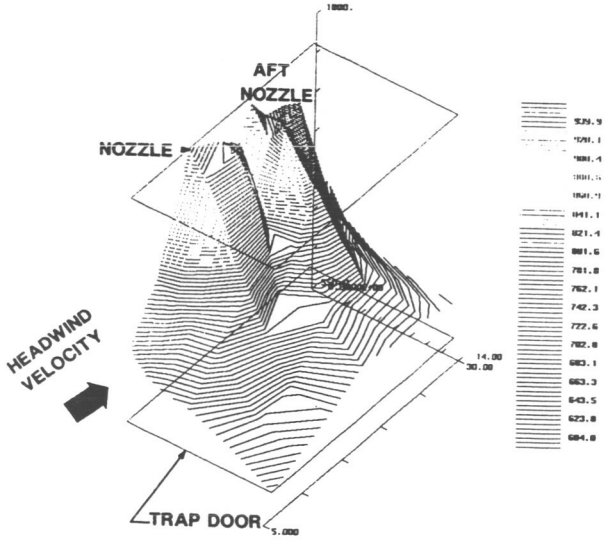

(a) TRAP DOOR.

FIGURE 22. - TYPICAL TRAP DOOR AND GROUND PLANE THREE-DIMENSIONAL SURFACE PLOTS AT 10 KNOTS AND NOZZLE PRESSURE RATIOS: FORWARD NOZZLES, 3.02; AFT NOZZLES, 3.16; COMPRESSOR FACE MACH NUMBER, 0.40; PITCH ANGLE, 6.5^{0}; AND MAIN LANDING GEAR HEIGHT (MODEL HEIGHT) ABOVE THE GROUND PLANE OF 0.20 IN.

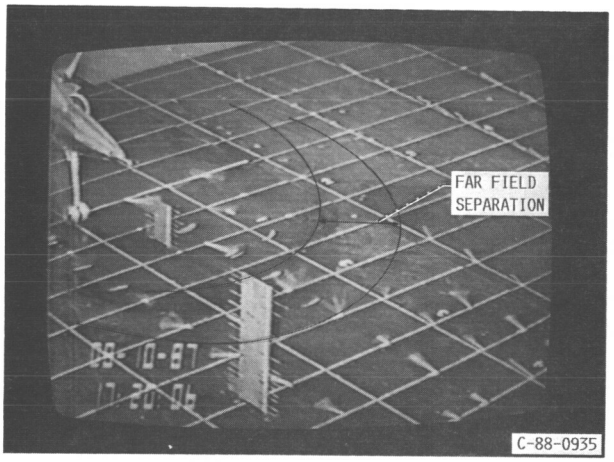

FIGURE 23. - FLOW VISUALIZATION VIEW SHOWING FAR FIELD SEPARATION AHEAD OF THE MODEL.

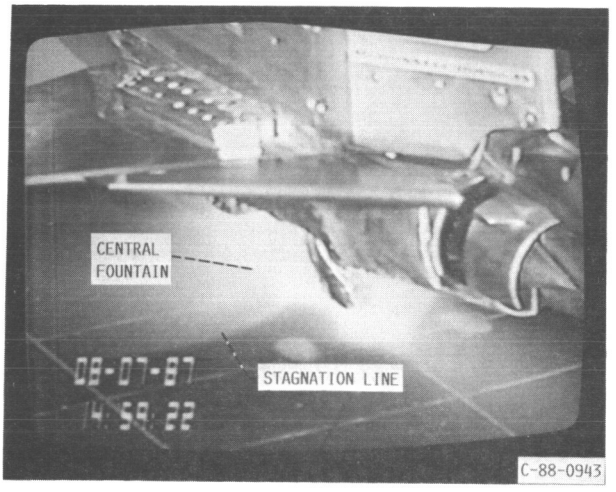

FIGURE 24. - THREE-QUARTER VIEW OF THE CLEAN CONFIGURATION SHOWING THE NEAR FIELD CENTRAL FOUNTAIN/LOCAL FLOW FIELD CHARACTERISTICS.

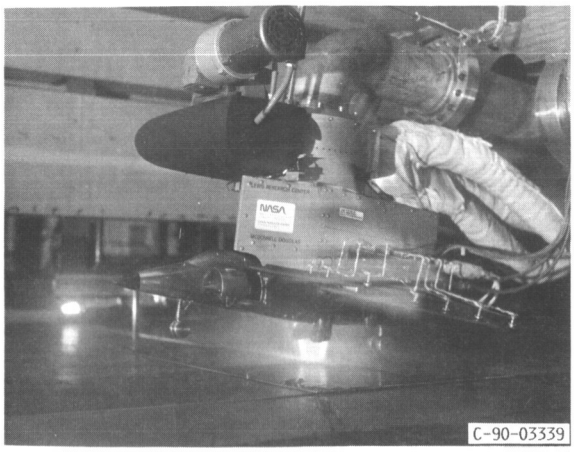

(a) FORWARD NOZZLES CENTERLINE STATION.

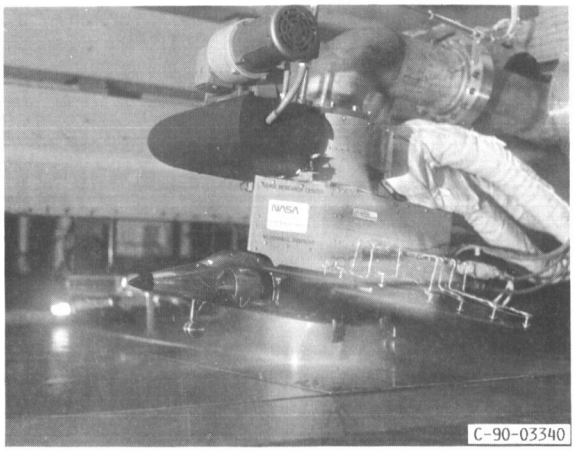

(b) AUXILIARY INLETS STATION.

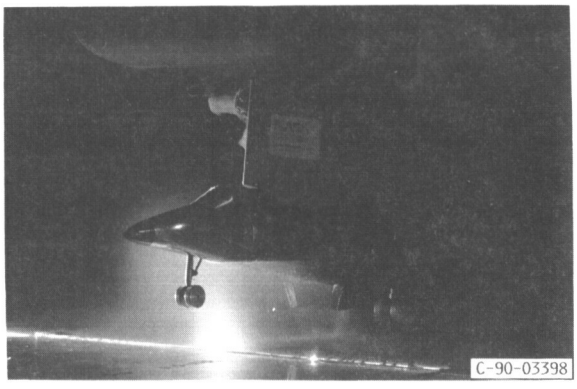

(c) MAIN INLET STATION.

FIGURE 25. - NEAR FIELD FLOW VISUALIZATION USING A LASER SHEET IN THE SPANWISE DIRECTION.

FIGURE 26. - FAR AND NEAR FIELD FLOW VISUALIZATION USING THE LASER SHEET IN THE STREAMWISE DIRECTION AT 10 KNOTS AND DESIGN CONDITIONS AT A MAIN LANDING GEAR HEIGHT OF 1.00 IN.

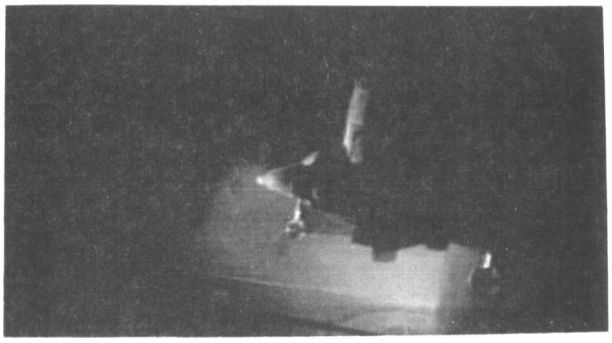

(a) VIDEO GRAY LEVEL OUTPUT.

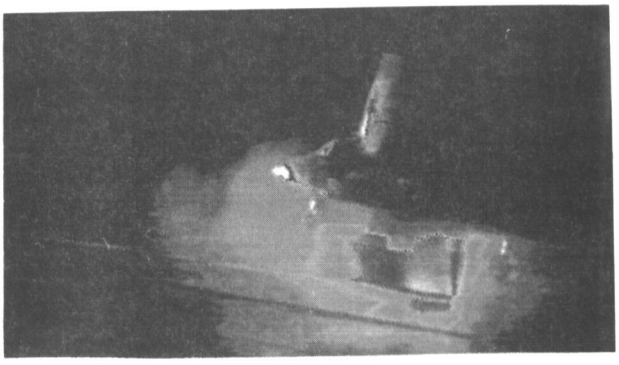

(b) COLOR ENHANCEMENT.

FIGURE 27. - LASER SHEET ILLUMINATION OF THE MODEL FLOW FIELD AT 23 KNOTS USING FALSE COLOR TO ENHANCE THE GRAY SCALE IN VIDEO IMAGE; NOZZLE PRESSURE RATIOS OF 1.74; COMPRESSOR FACE MACH NUMBER OF 0.40; AND A MAIN LANDING GEAR HEIGHT OF 12.00 IN. ABOVE THE GROUND PLANE.